DOI: 10.1002/ejic.200800315

Complex Hydrothermal Reaction Systems: A Systematic Investigation of Copper Phosphonatoethanesulfonates by High-Throughput Methods

Andreas Sonnauer[a] and Norbert Stock*[a]

Keywords: Metal phosphonatosulfonates / Inorganic-organic hybrid compounds / High-throughput methodology

The polyfunctional ligand 2-phosphonoethanesulfonic acid, $H_2O_3P–C_2H_4–SO_3H$ (H_3L), was used in a high-throughput (HT) investigation of a new class of compounds, the copper phosphonatosulfonates. An extensive HT study comprising 288 individual hydrothermal reactions was performed to systematically investigate the influence of temperature, pH, and molar ratio of Cu^{2+}/H_3L in the reaction system $Cu(NO_3)_2/H_3L/NaOH/H_2O$/temperature. The HT investigation led to five new compounds $Cu_2[(O_3P–C_2H_4–SO_3)(OH)(H_2O)](H_2O)$ (**1**), $Cu_{2.5}(O_3P–C_2H_4–SO_3)(OH)_2$ (**2**), $Cu_{1.5}[(O_3P–C_2H_4–SO_3)(H_2O)]·H_2O$ (**3**), $Cu_2[(O_3P–C_2H_4–SO_3)(OH)(H_2O)_2]·3H_2O$ (**4**), and $NaCu(O_3P–C_2H_4–SO_3)(H_2O)_3$ (**5**). Their fields of formation were established unequivocally and from the large amount of data reaction trends were extracted. Furthermore, a new compound $Cu_{1.5}(O_3P–C_2H_4–SO_3)(H_2O)$ (**6**) was synthesized under hydrothermal reaction conditions in a glass reactor. For compounds **1**, **2**, and **6** crystal structures were determined by single-crystal X-ray diffraction. The compounds exhibit a large structural variety. Thus, CuO_4, CuO_5, and CuO_6 units are observed. Corner-, edge- as well as face-sharing polyhedra form chains, layers, or Cu_3O_{12} clusters that are connected by the $–CH_2CH_2–$ group of the ligand. Thermogravimetric investigations, magnetic measurements, IR spectra as well as chemical analyses of compounds **1**, **3**, **4**, **5**, and **6** are also presented.

Introduction

The number of new inorganic–organic hybrid compounds is continuously increasing. These hybrid compounds can be classified depending on interactions and arrangement of the inorganic and organic building units.[1] The classes of inorganic–organic hybrids range from amorphous nanocomposites such as self-assembled mesoporous nanocomposites to crystalline hybrid materials. These compounds are mostly based on metal carboxylates, sulfonates, and phosphonates and are intensively investigated due to their potential applications as sorbents, ion exchangers, catalysts, or charge-storage materials.[2,3] Porous hybrid compounds based on metal carboxylates[4–6] and phosphonates[7–10] have attracted widespread interest in the past few years. We are interested in the use of organic ligands containing two or more different functional groups for the synthesis of functionalized porous hybrid compounds or bimetallic hybrid systems. Our focus lies on the investigation of the influence of geometry, coordination properties, charge, and acidity of the functional groups. In this respect, carboxylic acids differ strongly from functional groups such as phosphonic and sulfonic acids. Especially the presence of the third oxygen atom in phosphonic and sulfonic acids leads to a larger variety of coordination modes and very often pillared layered structures are obtained. So far our focus has been on the use of phosphonocarboxylic,[8] iminobis(methylphosphonic) $[(H_2O_3P–CH_2)_2N–CH_2C_6H_4–COOH]$[11] as well as tetra-phosphonic acids $[1,2,4,5\text{-}(H_2O_3PCH_2)_4C_6H_4]$.[12,13] Although a large number of metal phosphonates and metal sulfonates have been reported in the literature, compounds based on ligands containing simultaneously a phosphonic and a sulfonic acid group have only recently been investigated. These few studies are limited to the use of linker molecules based on rigid phosphonoarylsulfonic acids.[14–20] To the best of our knowledge only two investigations by our group using the flexible linker 2-phosphonethansulfonic acid have been reported in the literature.[21,22] In the course of our systematic investigation on the synthesis of inorganic–organic hybrid compounds based on $H_2PO_3–C_2H_4–SO_3H$ (H_3L) and di- as well as trivalent metal ions two series of isotypic lanthanide phosphonatosulfonates $Ln(O_3P–C_2H_4–SO_3)(H_2O)$[21] ($Ln$ = La–Dy) and $Ln(O_3P–C_2H_4–SO_3)$[23] (Ln = Ho–Lu, Y), as well as a barium phosphonatosulfonate $BaH(O_3P–C_2H_4–SO_3)$[22] have been obtained. We have now focused on the investigation of inorganic–organic hybrid compounds containing Cu^{2+} ions since these often exhibit interesting coordination geometries due to Jahn–Teller distortion. Furthermore, compounds containing uncoordinated copper sites, for example in water-free HKUST-1[24], are interesting for

[a] Institute of Inorganic Chemistry, Christian Albrechts University, Otto-Hahn-Platz 6/7, 24118 Kiel, Germany
Fax: +49-431-880-1775
E-mail: stock@ac.uni-kiel.de

Supporting information for this article is available on the WWW under http://www.eurjic.org or from the author.

catalytic or sensor applications. Therefore, a study on copper phosphonatosulfonates was started. Here we report the high-throughput study of the reaction system $Cu(NO_3)_2$/H_3L/NaOH/H_2O/temperature (T = 90 to 190 °C in steps of 20 °C, t = 48 h). The solvothermal investigation led to six new copper phosphonatosulfonates which were characterized in detail.

Results and Discussion

High-Throughput Investigation

The system $Cu(NO_3)_2$/H_3L/NaOH/H_2O/temperature was investigated using high-throughput methods. In the study five new compounds were identified. While **1** and **2** were obtained as single-crystalline products, compounds **3**, **4**, and **5** were isolated as microcrystalline products, which were characterized in detail using elemental and thermogravimetric analyses as well as IR spectroscopy. The results of the high-throughput experiment are based on powder XRD patterns and are shown in Figure 1. The following trends were observed focusing on reaction temperature and pH. The starting and ending pH of the individual reaction solutions were identical within the error margins. $Cu_2[(O_3P–C_2H_4–SO_3)(OH)(H_2O)](H_2O)$ (**1**) is mainly formed at temperatures from 130–190 °C. The compound is formed over a large region of molar ratios H_3L/Cu^{2+}/NaOH = 1:1:3, 2:1:4–5, 3:1:6–7, 1:2:4–5, 1:3:3–6, and 1:4:4–8 which correlates with the pH from approximately 3–7. Decreasing the temperature to 110 and 90 °C, compound **4** $Cu_2[(O_3P–C_2H_4–SO_3)(OH)(H_2O)_2]·3H_2O$ was formed under very similar compositional parameters (H_3L/Cu^{2+}/NaOH = 1:1:3, 2:1:5, 3:1:7, 4:1:10, 1:2:3–5, 1:3:3–7, 1:4:4–8). Compound **2** $Cu_{2.5}(O_3P–C_2H_4–SO_3)(OH)_2$ is obtained in the temperature range 130–190 °C and the reaction product is always contaminated with a microcrystalline by-product. This phase is only formed in the small pH range of pH 6–8, which corresponds to the molar ratios (H_3L/Cu^{2+}/NaOH = 1:1:3–4, 2:1:5–6, 4:1:10, 1:2:5–6, 1:3:7, 1:4:10). Decreasing the temperature to 110 and 90 °C, compound **5** $NaCu(O_3P–C_2H_4–SO_3)(H_2O)_3$ is formed in approximately the same field of formation (H_3L/Cu^{2+}/NaOH = 1:1:4, 2:1:5, 4:1:10, 1:2:6, 1:4:10) as compound **2**. Only $Cu_{1.5}[(O_3P–C_2H_4–SO_3)(H_2O)]·H_2O$ (**3**) was observed over the full temperature range from 90–190 °C but at more acidic conditions than previously described (pH = 2–3).

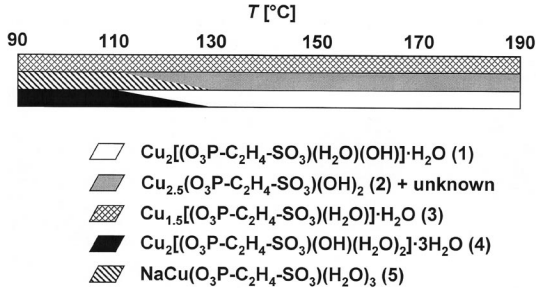

Figure 2. Extracted temperature-dependent fields of formation out of the high-throughput evaluation.

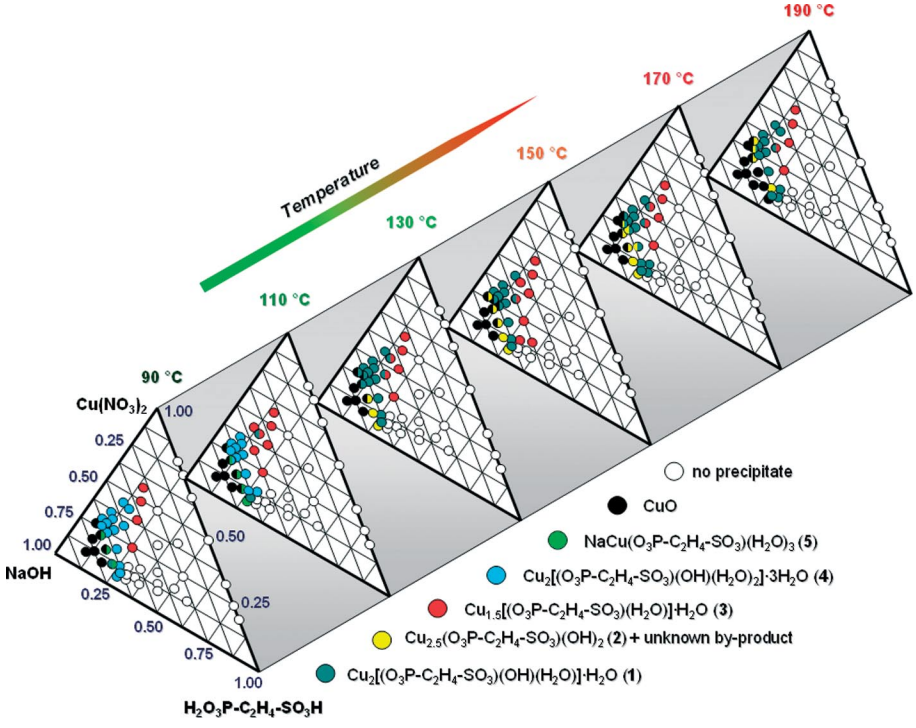

Figure 1. Crystallization diagram of the system $Cu(NO_3)_2$/$H_2O_3P–C_2H_4–SO_3H$/NaOH/H_2O/temperature. Results are based on powder XRD patterns. Phase-mixtures are indicated by dots with two or three colors.

This pH is observed at molar ratios Cu^{2+}/H_3L/NaOH = 1:1:2, 2:1:3–5, 1:2:2–3, 1:3:2–3, and 1:4:2–3. Basic conditions (pH ≈ 8) lead to the formation of traces of CuO in the mixtures. Stronger basic conditions with pH > 8 led always to the formation of CuO. These reaction trends are summarized in Figures 2 and 3, and show the formation of the title compounds in correlation with temperature and pH.

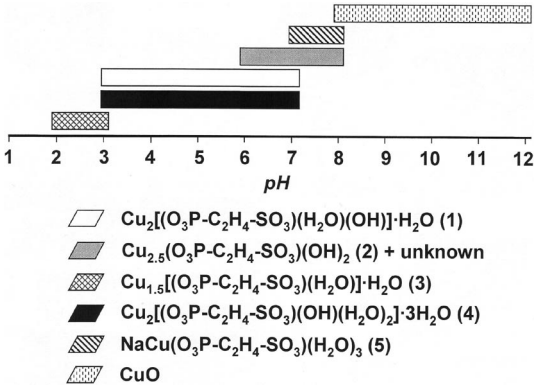

Figure 3. Extracted pH-dependent fields of formation. The starting and ending pH of the reactions were identical within the error margins.

Crystal Structure Determination

Because of the similar scattering factor of phosphorus and sulfur a distinction based on the structure refinement is not trivial. This can be unequivocally accomplished by comparing bond lengths with data reported in the literature. While in the copper phosphonates $Cu[HO_3PCH_2–C_6H_4–COOH]·2H_2O$[25] and $[\{Cu(H_2O)_2\}\ \{HO_3P(CH_2)_4PO_3H\}]_n$[26] P–O bond lengths in the range 151.2(2)–156.3(5) pm are observed, the corresponding S–O bond lengths in the copper sulfonates $Cu(O_3S–C_2H_4–SO_3)(H_2O)_4$[27] and $[Cu_2(C_7H_4O_5S)_2(C_{10}H_8N_2)_2(H_2O)_2]$[28] are significantly shorter 144.3(2)–146.6(1) pm. These values compare well with the bond lengths observed in our study where P–O and S–O distances of 151.9(3)–156.9(2) pm and 144.9(3)–148.7(2) pm, respectively, are observed. The simulated and measured powder XRD patterns for **1**, **2**, and **6** compare well (Figure S1 in the Supporting Information).

Crystal Structure of $Cu_2[(O_3P–C_2H_4–SO_3)(OH)(H_2O)]·H_2O$ (1)

The structure is composed of three Cu^{2+} ions (Cu1, Cu2, Cu3) and one 2-phosphonatoethanesulfonate $(O_3P–C_2H_4–SO_3)^{3–}$ ion, as well as water molecules (O8 coordinated, O9 uncoordinated) and one hydroxide ion (O7). Each copper ion is surrounded by six oxygen atoms. The copper ions Cu1 and Cu3 are coordinated by four $O_3P–C_2H_4–SO_3^{3–}$ ions each through two S–O–Cu and P–O–Cu bonds. The full coordination spheres are completed by two hydroxide ions O7. The surrounding of Cu2 is formed through three P–O–Cu bonds and one S–O–Cu bond from the 2-phosphonatoethanesulfonate ion, as well as one hydroxide O7 and one water molecule O9. The oxygen atoms act as end on (O3, O4, O5, O6, O8) as well as bridging ligand atoms (μ-O1, μ-O2, μ_3-O7). Thus, edge-sharing CuO_6 polyhedra are observed, that lead to the formation of zigzag chains along the *a* axis (Figure 4). These chains are connected to layers by the phosphonate and sulfonate groups. The interconnection of the layers is accomplished through the $–CH_2–CH_2–$ groups of the ligand and a three-dimensional framework is formed (Figure 5). The resulting small pores are occupied by noncoordinating water molecules. The structure collapses irreversibly upon the removal of the water molecules. The hydrogen atoms of the hydroxide ion O7 and the water molecules O8 and O9 could not be located in the difference Fourier map. However, the interatomic distances O8···O5 [2.824(6)], O8···O6 [2.806(7)], O9···O2 [2.995(6)], and O9···O8 [2.673(7)] indicate the presence of hydrogen bonds. The proposed hydrogen bonding scheme is given in Figure 6.

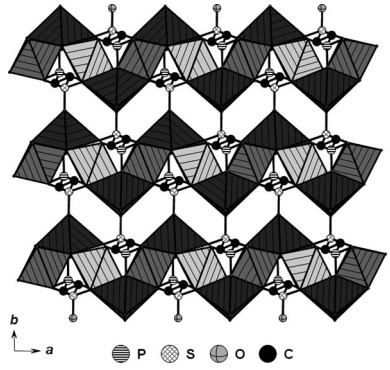

Figure 4. Infinite zigzag chains of edge-sharing CuO_6 polyhedra along the *a* axis in $Cu_2[(O_3P–C_2H_4–SO_3)(OH)(H_2O)]·H_2O$ (**1**). CuO_6 polyhedra are shaded in gray (Cu1 middle, Cu2 dark, Cu3 light). For sake of clarity H-atoms connected to C-atoms are omitted.

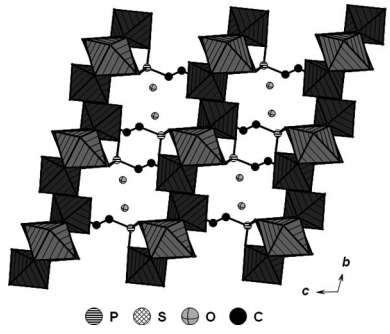

Figure 5. The zigzag chains of edge-sharing CuO_6 polyhedra in compound **1** are connected to layers by the phosphonate and sulfonate groups. The interconnection of the layers is accomplished through the $–CH_2–CH_2–$ groups of the ligand into a three-dimensional framework. CuO_6 polyhedra are shaded in gray (Cu1 middle, Cu2 dark, Cu3 light). The resulting small pores are occupied by uncoordinating water molecules. For sake of clarity H-atoms connected to C-atoms are omitted.

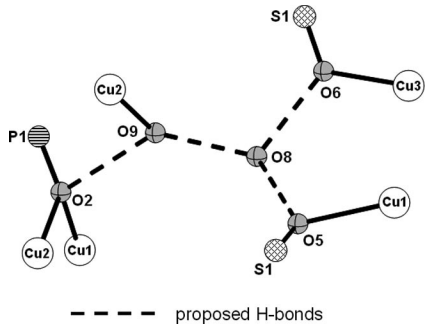

Figure 6. Proposed H-bonding scheme in the structure of compound **1**. The hydrogen atoms could not be located in the difference Fourier map.

Crystal Structure of $Cu_{2.5}(O_3P–C_2H_4–SO_3)(OH)_2$ (2)

The framework includes four crystallographically independent Cu^{2+} ions (Cu1, Cu2, Cu3, Cu4), and one 2-phosphonatoethanesulfonate $(O_3P–C_2H_4–SO_3)^{3-}$ ion, as well as two hydroxide ions (O7, O8). Each copper ion is surrounded by six oxygen atoms. The copper ions Cu2, Cu3, and Cu4 are coordinated by four $O_3P–C_2H_4–SO_3^{3-}$ ions each through two P–O–Cu and S–O–Cu bonds. Each coordination sphere is completed by two hydroxide ions for Cu2 ($2 \times O8$) and for Cu3 as well as Cu4 ($2 \times O7$). The oxygen atoms act as end on (O3) as well as bridging ligand atoms (μ-O1, μ-O2, μ-O5, μ-O6, μ_3-O7, μ_3-O8). Thus, corner-, edge-, and face-sharing CuO_6 polyhedra are observed which form an extended M–O–M layer in the *ac* plane (Figure 7, a). These layers are connected through the $–CH_2–CH_2–$ groups into a three-dimensional pillared framework (Figure 7, b). Only the hydrogen atom for the hydroxide ion O8 could be unequivocally located in the difference Fourier map. It acts as an H-donor in the hydrogen bond with the uncoordinated oxygen atom O4 of the sulfonate group [O8···O4 distance: 274.2(4) pm]. The short interatomic distance O7···O4 of 284.3(4) pm indicates a second hydrogen bond of O4 as H-acceptor with O7 as H-donor (Figure 8). A short Cu–Cu distance of 275.4(1) pm is observed between the face sharing $Cu3O_6$ and $Cu4O_6$ polyhedra. These polyhedra form a one-dimensional chain along the *a* axis (Figure 9).

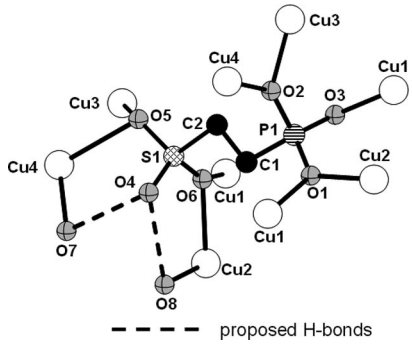

Figure 8. Proposed H-bonding scheme in the structure of compound **2**.

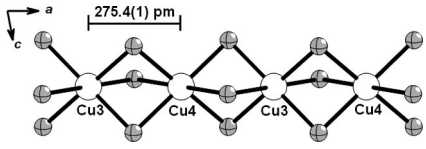

Figure 9. In $Cu_{2.5}(O_3P–C_2H_4–SO_3)(OH)_2$ (**2**) short interatomic distances between Cu3 and Cu4 of 275.4(1) pm are observed. In the corresponding M–O–M network Cu3 and Cu4 form one-dimensional chains along the *a* axis.

Crystal Structure of $Cu_{1.5}(O_3P–C_2H_4–SO_3)(H_2O)$ (6)

The compound is composed of two Cu^{2+} ions (Cu1, Cu2), and one 2-phosphonatoethanesulfonate $(O_3P–C_2H_4–SO_3)^{3-}$ ion, as well as one water molecule (O7). The copper ion Cu1 is coordinated through four P–O–Cu bonds and forms a square-planar CuO_4 unit. The Cu2 ion is surrounded by two P–O–Cu and S–O–Cu bonds each. The co-

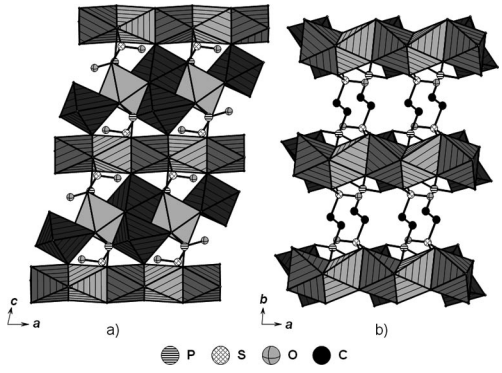

Figure 7. a) Corner-, edge-, and face-sharing CuO_6 polyhedra in $Cu_{2.5}(O_3P–C_2H_4–SO_3)(OH)_2$ (**2**) form M–O–M layers in the *ac* plane. b) These M–O–M layers are connected by the $–CH_2–CH_2–$ groups to a three-dimensional framework. CuO_6 polyhedra are shaded in gray (Cu1 dark, Cu2 no hatching, Cu3 middle, Cu4 light). For sake of clarity H-atoms are omitted.

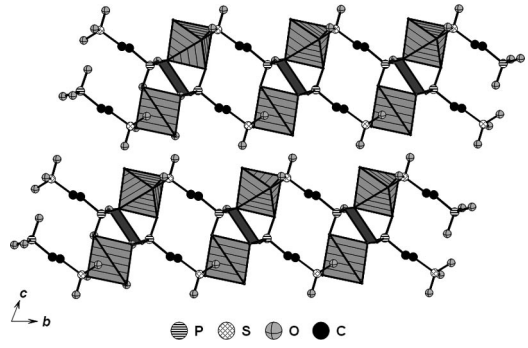

Figure 10. Compound **6** contains CuO_4 and CuO_5 units which form Cu_3O_{12} clusters. These trimeric clusters are interconnected by the $–CH_2CH_2–$ groups to double layers, which form a three-dimensional framework by hydrogen bonds. CuO_4 planes and CuO_5 polyhedra are shaded in gray. For sake of clarity H-atoms are omitted.

Table 1. Refined cell parameters[29] of the powder XRD patterns of compounds **3**, **4**, and **5**.

Parameter	**3**	**4**	**5**
Chemical formula	$C_2H_8Cu_{1.5}O_8PS$	$C_2H_{15}Cu_2O_{12}PS$	$C_2H_{10}CuNaO_9PS$
Formula weight	318.44	421.27	327.67
Crystal system	triclinic	monoclinic	monoclinic
a [pm]	1074.7(2)	1579.7(6)	1625.2(5)
b [pm]	849.1(2)	715.8(2)	767.9(2)
c [pm]	509.6(1)	1057.0(3)	748.9(2)
α [°]	78.67(1)	90	90
β [°]	101.95(1)	105.03(2)	114.86(1)
γ [°]	115.02(1)	90	90
V (10^6 pm^3)	409.1(2)	1154(1)	848.0(5)
Figure of merit	*F*(30) = 73.9 (0.007, 61)	*F*(30) = 45.3 (0.007, 97)	*F*(30) = 39.3 (0.008, 107)

ordination sphere is completed by the water molecule O7. The oxygen atoms act as end on (O2, O3, O4, O5, O6, O7) as well as bridging ligand atoms (μ-O1). One CuO_4 unit is linked to two CuO_5 units and trimeric Cu_3O_{12} clusters are formed. These clusters are interconnected by the $–CH_2CH_2–$ groups to double layers in the *ab* plane, which are further connected by hydrogen bonds between the water molecule O7 and oxygen atoms (O4, O5) of the sulfonate group (Figure 10). The hydrogen atoms of the water molecule could be unequivocally located in the difference Fourier map and act as H-donors. H-acceptors are the O4 and O5 atoms of the sulfonate group.

Characterization of Compounds 3, 4, and 5

While compounds **1**, **2**, and **6** were obtained as coarse crystalline products, **3**, **4**, and **5** were only isolated as microcrystalline compounds. Therefore, **3**, **4**, and **5** were characterized thoroughly by powder XRD (Figure S2). The powder XRD patterns were indexed and refined with the STOE WinXPOW program using the Louer's algorithm (DICVOL).[29] The refined cell parameters are summarized in Table 1. The compositions were determined based on thermogravimetric (TG), CHNS, and Energy Dispersive X-ray (EDX) analyses. $Cu_{1.5}[(O_3P–C_2H_4–SO_3)(H_2O)]·H_2O$ (**3**), M = 318.44 g mol^{-1}: EDX measurement: atomic ratio P/S/Cu = 1:1:1.6; found C 7.68, H 2.47, S 9.76; calcd. C 7.55, H 2.53, S 10.07. $Cu_2[(O_3P–C_2H_4–SO_3)(OH)(H_2O)_2]·3H_2O$ (**4**), M = 421.27 g mol^{-1}: EDX measurement: atomic ratio P/S/Cu = 1:1:2.1; found C 5.74, H 3.47, S 7.72; calcd. C 5.70, H 3.59, S 7.61. $NaCu(O_3P–C_2H_4–SO_3)(H_2O)_3$ (**5**), M = 327.67 g mol^{-1}: EDX measurement: atomic ratio P/S/Cu/Na = 1:1:1:1; found C 7.87, H 2.51, S 9.94; calcd. C 7.53, H 2.76, S 9.73.

IR Spectroscopy

The title compounds were studied by IR spectroscopy (Figure S3). All compounds exhibit typical bands in the region between 1300 and 950 cm^{-1} that are due to the stretching vibrations of the $CPO_3–$ and the $CSO_3–$ groups; however, the individual bands cannot be assigned unambiguously. Bands in the region from 2960 to 2920 cm^{-1} are due to C–H stretching vibrations. The corresponding CH_2 deformation vibrations appear in the region between 1405 and 1420 cm^{-1}. All compounds exhibit several broad bands in the region between 3600 and 3070 cm^{-1}, due to extensive hydrogen bonding.

Thermal Study

For information on the thermal stability of the compounds **1**, **3**, **4**, **5**, and **6** thermogravimetric measurements (Figure S4) were performed and the results are summarized in Table 2. All investigated compounds contain H_2O molecules. On the basis of the dehydration temperature coordi-

Table 2. Summary of the results of the thermogravimetric investigations for $Cu_2[(O_3P–C_2H_4–SO_3)(OH)(H_2O)](H_2O)$ (**1**), $Cu_{1.5}[(O_3P–C_2H_4–SO_3)(H_2O)]·H_2O$ (**3**), $Cu_2[(O_3P–C_2H_4–SO_3)(OH)(H_2O)_2]·3H_2O$ (**4**), $NaCu(O_3P–C_2H_4–SO_3)(H_2O)_3$ (**5**), and $Cu_{1.5}(O_3P–C_2H_4–SO_3)(H_2O)$ (**6**). The TG curves are shown in Figure S4 in the Supporting Information.

Compound	**1**	**3**	**4**	**5**	**6**
Total number of H_2O molecules	2	2	5	3	1
Number of uncoordinated H_2O	1[b]	1	3	[a]	–
Temperature range [°C]	30–300	30–90	30–95	30–190	–
Weight loss: obsd./calcd. [wt.-%]	[a]	–5.7/–5.7	–12.1/–12.8	[a]	–
Number of coordinated H_2O	1[b]	1	2	3	1[b]
Temperature-range [°C]	30–300	140–240	250–320	30–190	150–250
Weight loss: obsd./calcd. [wt.-%]	–8.8[c]/–9.8[c]	–5.5/–5.7	–9.4/–8.6	–17.5/–16.5	–6.2/–6.0
Decomposition temperature [°C]	>320	>400	>320	>320	>350

[a] Coordinated and uncoordinated water molecules could not be clearly distinguished. [b] Number of water molecules based on the results of the single-crystal structure determination. [c] The difference between the observed and calculated water content results from the loss of uncoordinated water at room temperature.

nated and uncoordinated water molecules can be distinguished. The decomposition temperature of the organic linker depends on the structure of the copper phosphonatosulfonates and values between 320 and 400 °C are observed.

Magnetic Property Study

All compounds except for **2** were studied by magnetic measurement (Figure S5 shows the magnetic susceptibility χ, inverse susceptibility χ^{-1} and $\chi \cdot T$ plotted as a function of temperature from 2–300 K). The compounds **1**, **3**, **4**, **5**, and **6** exhibit Curie–Weiss behavior in the ranges 80–300 K, 140–300 K, 140–300 K, 10–300 K, and 6–300 K, respectively. The data of **1**, **3**, **4**, and **6** were least-square fitted by the Curie–Weiss equation $\chi_M = C/(T - \theta)$ (**1**: C = 0.73 K cm^3 mol^{-1}, θ = –22.4 K; **3**: C = 0.73 K cm^3 mol^{-1}, θ = –21.0 K; **4**: C = 0.69 K cm^3 mol^{-1}, θ = 17.0 K; **6**: C = 0.58 K cm^3 mol^{-1}, θ = –9.8 K). The data of compound **5** were nonlinear fitted with the equation $\chi_M = C/(T - \theta) + \chi_0$, which includes the temperature-independent paramagnetic factor χ_0 (**5**: C = 0.35 K cm^3 mol^{-1}, θ = –0.7 K, χ_0 = 5.94×10^{-4} cm^3 mol^{-1}). The effective magnetic moments (**1**: 1.7 B.M.; **3**: 1.7 B.M.; **4**: 1.7 B.M.; **5**: 1.7 B.M; **6**: 1.8 B.M.) compare well with values observed for Cu^{2+} ions (1.7–2.2 B.M.). The $\chi \cdot T$ vs. T plots of the compounds **1** and **4** show similar temperature dependence. For **1** at temperatures above 25 K antiferromagnetic interactions dominate, which change to ferro/ferrimagnetic and finally at low temperatures (<6 K) again to antiferromagnetic interactions. In compound **4** ferro/ferrimagnetic interactions dominate down to 100 K, which change to antiferromagnetic and then to ferro/ferrimagnetic interactions. At low temperatures (<4 K) a change to antiferromagnetic interactions is observed as in **1**. Compound **1** contains zigzag chains of Cu–O–Cu edge-sharing polyhedra. Because of the similarity of the $\chi \cdot T$ vs. T plots compound **4** may also contain this M–O–M motif. This unusual behavior could be due to slight temperature-dependent anisotropic structural changes. The $\chi \cdot T$ vs. T plots of the compounds **3**, **5**, and **6** indicate antiferromagnetic interactions at low temperatures (<50 K).

Discussion

The structural chemistry of metal phosphonatosulfonates is strongly determined by the flexibility of the ligand and the presence of additional co-ligands during the synthesis. The use of rigid phosphonosulfonic acids, i.e. phosphonoarylsulfonic acids, together with phen or bipy ligands leads to di-, tetra-, or hexanuclear metal-phosphonoarylsulfonate clusters. Up to now, only the chemistry of M = Ln^{3+},[15] Zn^{2+},[16] Mn^{2+}[19], and Cd^{2+}[20] have been investigated in these systems. In contrast to the rigid systems, the flexible phosphonoethanesulfonic acid has yielded compounds with extended M–O–M structures. Layers (**2**), chains [**1**, $Ln(O_3P–C_2H_4–SO_3)(H_2O)$,[21] $BaH(O_3P–C_2H_4–SO_3)$[22]], and a trimeric cluster (compound **6**), as well as isolated M–O polyhedra in $Er(O_3P–C_2H_4–SO_3)$[23] have been observed. The formation of extended M–O–M structures has also been reported with flexible di-phosphonic acids. Thus, $Cu_2[(O_3P–C_4H_8–PO_3)(H_2O)_2]\cdot 2H_2O$ and $Cu_2[(O_3P–C_5H_{10}–PO_3)(H_2O)_2]\cdot 2.8H_2O$ contain extended M–O–M chains of $CuO_4(OH)_2$ octahedra, which are bridged by the phosphonate groups to layers and cross-linked by the alkyl chains into a three-dimensional framework.[30] Pillared layered structures were found in the copper phosphonates $Cu_2[(O_3P–C_2H_4–PO_3)(H_2O)_2]$ and $Cu_2[(O_3P–C_3H_6–PO_3)(H_2O)_2]\cdot H_2O$ where chains of edge- and corner-sharing polyhedra, respectively, are linked by the phosphonate groups to layers, which are connected by the alkyl chains into three-dimensional frameworks.[31] Infinite M–O–M zigzag chains of CuO_5 polyhedra were observed in $Cu_2(O_3P–CH_2–PO_3)$.[32] These compounds based on flexible alkyl ligands are structurally related to the copper phosphonatoethanesulfonates of this study due to the pillared construction of the frameworks. In all these copper phosphonates each oxygen atom of the phosphonate group coordinates at least to one copper ion. Because of the reduced ionic charge of the phosphonosulfonic acid in comparison to the di-phosphonic acid in our metal phosphonatosulfonates frequently only two oxygen atoms of the sulfonate groups are coordinated to metal ions. The third oxygen is involved in the formation of hydrogen bonds. This reduced coordination of the sulfonate group is observed in $Cu_{2.5}(O_3P–C_2H_4–SO_3)(OH)_2$ (**2**), $Cu_{1.5}(O_3P–C_2H_4–SO_3)(H_2O)$ (**6**), and $Ln(O_3P–C_2H_4–SO_3)(H_2O)$.[21]

Conclusions

Five new compounds $Cu_2[(O_3P–C_2H_4–SO_3)(OH)(H_2O)](H_2O)$ (**1**), $Cu_{2.5}(O_3P–C_2H_4–SO_3)(OH)_2$ (**2**), $Cu_{1.5}[(O_3P–C_2H_4–SO_3)(H_2O)]\cdot H_2O$ (**3**), $Cu_2[(O_3P–C_2H_4–SO_3)(OH)(H_2O)_2]\cdot 3H_2O$ (**4**), and $NaCu(O_3P–C_2H_4–SO_3)(H_2O)_3$ (**5**) were synthesized in the high-throughput investigation of the system $Cu(NO_3)_2/H_3L$/NaOH/H_2O/temperature (T = 90 to 190 °C in steps of 20 °C, t = 48 h). The evaluation of the HT experiment led to the determination of the fields of formation. On the basis of these results, temperature- and pH-dependent reaction trends were extracted. Thus, the outcome of a reaction can be "predicted" with a high probability within the investigated parameter space based on temperature and pH. This was proven in additional experiments several times with high reproducibility. Furthermore, structural trends were determined. Higher reaction temperatures lead to compounds with lower water content and higher reaction pH results in the formation of higher condensed M–O structures. The synthesized compounds exhibit infinite M–O–M zigzag chains of CuO_6 polyhedra in $Cu_2[(O_3P–C_2H_4–SO_3)(OH)(H_2O)](H_2O)$ (**1**) and extended M–O–M layers of corner-, edge-, and face-sharing CuO_6 polyhedra in $Cu_{2.5}(O_3P–C_2H_4–SO_3)(OH)_2$ (**2**). Our high-throughput methodology is an excellent tool for detailed investigations of solvothermal reaction systems and allows the determination of the fields of formation, as well as reaction and structural trends.

Experimental Section

Materials and Methods: 2-Phosphonoethanesulfonic acid (H_3L) was synthesized as previously reported in a two-step nucleophilic substitution reaction with triethylphosphite and sodium sulfite starting from 1,2-dibromoethane.[22] All other reagents were of analytical grade (Aldrich and Fluka) and were used without further purification. High-throughput X-ray analyses were carried out in transmission geometry using a STOE high-throughput powder diffractometer equipped with a linear position-sensitive detector (PSD) system.[33] MIR spectra were recorded with an ATI Matheson Genesis in the spectral range 4000–400 cm^{-1} using the KBr disk method. Thermogravimetric analyses were carried out in nitrogen (75 mL min^{-1}, 30–700 °C, 4 °C min^{-1}) using a NETSCH STA 409 CD Analyzer. CHNS analyses were performed with a Eurovektor EuroEA Elemental Analyzer. The semiquantitative elemental analyses were performed with a Phillips ESEM XL 30 hot cathode scanning electron microscope equipped with an energy dispersive X-ray (EDX) EDAX analyzer for elemental analysis. Magnetic measurements for compounds **1**, **3**, and **4** were performed with a Lake Shore Cryomatic AC-susceptometer 7000 at 10 kOe (DC-field) in the temperature range from 2–300 K (ZFC). For compounds **5** and **6** the magnetic measurements were performed with a SQUID magnetometer MPMS-XL5 from Quantum Design Inc. using identical field and temperature parameters as for **1**, **3**, and **4**.

High-Throughput Experiments: The reaction system $Cu(NO_3)_2$/H_3L/NaOH/H_2O/temperature was investigated at six temperatures (90, 110, 130, 150, 170, and 190 °C) using high-throughput methods (reaction time: 48 h). Each HT experiment was performed under hydrothermal conditions in a custom-made high-throughput reactor system containing 48 PTFE inserts each with a maximum volume of 300 μL.[21,34] The process parameters, except for the temperature, were identical for all HT experiments and seven molar ratios Cu^{2+}: H_3L (1:1, 1:2, 1:3, 1:4, 2:1, 3:1, and 4:1) were used. The NaOH content was increased in different steps from 0–10 mol equivalents based on the amount of H_3L. Each reaction contained the identical amount of H_3L (0.053 mmol). The evaluation of the HT experiments based on powder XRD patterns is given in Figure 1. Exact amounts of starting materials are given in Table S1 in the Supporting Information.

Scale-Up Synthesis of $Cu_2[(O_3P–C_2H_4–SO_3)(OH)(H_2O)](H_2O)$ (1): Larger amounts of compound **1** were obtained using a glass reactor (DURAN culture tubes 12 × 100 mm D50 GL 14 M.KAP, SCHOTT 261351155). Aqueous solutions of 2.0 M H_3L (263 μL, 0.53 mmol), 2.0 M $Cu(NO_3)_2$ (536 μL, 1.06 mmol), and 2.0 M NaOH (1053 μL, 2.12 mmol) were combined and H_2O was added to give the final volume (2500 μL). The mixture was heated at 150 °C for 16 h. The yielded greenish solid (158 mg, 81% based on H_3L) was identified by powder X-ray diffraction.

Synthesis of $Cu_{1.5}[(O_3P–C_2H_4–SO_3)(H_2O)]·H_2O$ (3): The synthesis of compound **3** could not be scaled-up in glass or Teflon® reactors. Pure phase product was collected from Teflon® reactors of a separate high-throughput experiment. The HT experiment contained 48 identical reaction mixtures with the molar ratio H_3L/Cu^{2+}/NaOH = 1:2:2. Each reactor was filled with aqueous solutions of 2.0-M H_3L (26.3 μL), 2.0-M $Cu(NO_3)_2$ (52.6 μL), 2.0-M NaOH (52.6 μL), and H_2O (68 μL). The mixtures were heated at 110 °C for 48 h. The reaction products were characterized by powder X-ray diffraction [yield: 60 mg (%) based on H_3L].

Scale-Up Synthesis of $Cu_2[(O_3P–C_2H_4–SO_3)(OH)(H_2O)_2]·3H_2O$ (4): The synthesis of compound **4** was scaled-up in a glass reactor (DURAN culture tubes 12 × 100 mm D50 GL 14 M.KAP, SCHOTT 261351155). 2.0 M H_3L (263 μL, 0.53 mmol), 2.0 M $Cu(NO_3)_2$ (536 μL, 1.06 mmol), and 2.0 M NaOH (789 μL, 1.59 mmol) were combined and H_2O was added to give the final volume (2500 μL). The mixture was heated at 90 °C for 16 h. The yielded white-blue solid (83 mg, 37% based on H_3L) was identified by powder X-ray diffraction.

Synthesis of $NaCu(O_3P–C_2H_4–SO_3)(H_2O)_3$ (5): As observed for compound **3** the synthesis of **5** could not be scaled-up in glass or Teflon® reactors. Pure phase product was also collected from a separate high-throughput experiment. The HT experiment contains 48 identical reaction mixtures with the molar ratio H_3L/Cu^{2+}/NaOH = 4:1:10. Each reactor was filled with aqueous solutions of 2.0 M H_3L (26.3 μL), 2.0 M $Cu(NO_3)_2$ (13.2 μL), 1.0 M NaOH (65.8 μL), and H_2O (95 μL). The mixtures were heated at 110 °C for 48 h. The reaction products were characterized by powder X-ray diffraction. Because of the small field of formation (Figure 1), the synthesis is very sensitive to the reaction conditions and the

Table 3. Crystal data for compounds **1**, **2**, and **6**.

Parameter	**1**[a]	**2**	**6**
Chemical formula	$C_2H_9Cu_2O_9PS$	$C_2H_6Cu_{2.5}O_8PS$	$C_2H_6Cu_{1.5}O_7PS$
Crystal system	triclinic	triclinic	triclinic
Space group	$P\bar{1}$	$P\bar{1}$	$P\bar{1}$
a [pm]	711.54(14)	550.89(11)	510.72(10)
b [pm]	742.40(15)	831.29(17)	784.85(16)
c [pm]	882.17(18)	955.76(19)	1028.5(2)
α [°]	109.36(3)	75.62(3)	71.40(3)
β [°]	95.13(3)	78.01(3)	87.38(3)
γ [°]	90.52(3)	83.88(3)	80.58(3)
V [10^6 pm^3]	437.52(15)	414.03(14)	385.46(13)
Z	2	2	2
Formula weight	367.20	379.95	300.41
Total number of data collected	3241	4452	4497
Unique/obsd. data [$I > 2\sigma(I)$]	1306/1075	1926/1585	2226/1919
R(int.)	0.0514	0.0369	0.0668
*R*1, *wR*2 [$I > 2\sigma(I)$]	0.0346, 0.0902	0.0314, 0.0832	0.0304, 0.0772
*R*1, *wR*2 (all data)	0.0441, 0.0941	0.0419, 0.0866	0.0364, 0.0799
GOF	1.024	0.998	1.033
Δ*e* min./max. [e·$Å^{-3}$]	–0.640/0.783	–1.125/1.146	–0.823/0.585

[a] Compound **1** is nonmerohedral twinned.

pre-treatment of the Teflon® reactors. Pure phase product with a total mass of 20 mg (yield: 14% based on H_3L) was obtained.

Synthesis of $Cu_{1.5}(O_3P–C_2H_4–SO_3)(H_2O)$ (6): The synthesis of **6** is very sensitive to small parameter variations. Pure phase material of **6** was only obtained using a glass reactor (DURAN culture tubes 12 × 100 mm D50 GL 14 M.KAP, SCHOTT 261351155). A mixture of 2.0 M H_3L (394 μL, 0.79 mmol), 2.0 M $Cu(NO_3)_2$ (789 μL, 1.58 mmol), 2.0 M NaOH (170 μL, 0.34 mmol), and H_2O (1500 μL) was filled into the culture tube. The mixture was homogenized by shaking for two minutes and heated at 170 °C for 36 h under hydrothermal conditions. Light blue rod-shaped crystals were collected with 15% yield based on H_3L.

X-ray Crystallography: Suitable crystals of the compounds $Cu_2[(O_3P–C_2H_4–SO_3)(OH)(H_2O)]·H_2O$ (**1**), $Cu_{2.5}(O_3P–C_2H_4–SO_3)(OH)_2$ (**2**), and $Cu_{1.5}(O_3P–C_2H_4–SO_3)(H_2O)$ (**6**) were carefully selected from the HT experiments using a polarizing microscope. Single-crystal X-ray diffraction experiments were performed with a STOE IPDS-1 diffractometer equipped with a fine-focus sealed tube (Mo-K_α radiation, λ = 71.073 pm). For data reduction and absorption correction the program XRED was used.[35]

The single crystal structures were solved by direct methods and refined using the program package SHELXTL.[36] The crystal of compound **1** is nonmerohedral twinned. The reflections of both individuals were indexed separately using RECIPE and integration of the intensities was performed using TWIN.[35] By this procedure, overlapping reflections are omitted. All hydrogen atoms of the $–CH_2–$ groups were placed onto calculated positions. For compounds **2** and **6**, hydrogen atoms of hydroxide ions and water molecules could be unequivocally localized from the difference Fourier map, the hydrogen bond lengths and angles are given in Table S2 (see Supporting Information). Experimental data and results of the structure determination of compounds **1**, **2**, and **6** are given in Table 3. Selected bond lengths are summarized in the Table S3.

CCDC-680739 (for **1**), -680741 (for **2**), and -680740 (for **6**) contain the supplementary crystallographic data for this paper. These data can be obtained free of charge from The Cambridge Crystallographic Data Centre via www.ccdc.cam.ac.uk/data_request/cif.

Supporting Information (see also the footnote on the first page of this article): Detailed reaction parameters of the high-throughput investigation, powder X-ray diffraction patterns for all compounds, IR spectra, magnetic measurement plots, and TG measurements for **1**, **3**, **4**, **5**, and **6** as well as X-ray crystallographic files in CIF format of **1**, **2**, and **6**. Additionally a comparison of the measured and simulated XRD pattern of **1**, **2**, and **6** are given.

Acknowledgments

The authors thank Priv.-Doz. Dr. Christian Näther for the acquisition of the single-crystal data, Inke Jess for TG measurements, Daniel Bichler, Maren Rassmusen, and Henning Lühmann for magnetic measurements. This work was supported by the Deutsche Forschungsgemeinschaft (DFG) (STO 643/2-2).

[1] C. Sanchez, B. Julian, P. Belleville, M. Popall, *J. Mater. Chem.* **2005**, *15*, 3559–3592.
[2] A. Clearfield, "Metal Phosphonate Chemistry" in *Progress in Inorganic Chemistry* (Ed. K. D. Karlin), Wiley, New York, **1998**, vol. 47, pp. 371.
[3] A. K. Cheetham, G. Férey, T. Loiseau, *Angew. Chem. Int. Ed.* **1999**, *38*, 3268–3292.
[4] H. Li, M. Eddaoudi, M. O'Keeffe, O. M. Yaghi, *Nature* **1999**, *402*, 276–279.
[5] M. Latroche, S. Suble, C. Serre, C. Mellot-Draznieks, P. L. Llewellyn, J. Lee, J. Chang, S. H. Jhung, G. Férey, *Angew. Chem. Int. Ed.* **2006**, *45*, 8227–8231.
[6] E. Biemmi, T. Bein, N. Stock, *Solid State Sci.* **2006**, *8*, 363–370.
[7] C. Serre, J. A. Groves, P. Lightfoot, A. M. Z. Slawin, P. A. Wright, N. Stock, T. Bein, M. Haouas, F. Taulelle, G. Férey, *Chem. Mater.* **2006**, *18*, 1451–1457.
[8] S. Bauer, H. Müller, T. Bein, N. Stock, *Inorg. Chem.* **2005**, *44*, 9464–9470.
[9] E. Brunet, M. José de la Mata, O. Juanes, J. C. Rodríguez-Ubis, *Angew. Chem. Int. Ed.* **2004**, *43*, 619–621.
[10] E. Brunet, M. José de la Mata, H. M. H. Alhendawi, C. Cerro, M. Alonso, O. Juanes, J. C. Rodríguez-Ubis, *Chem. Mater.* **2005**, *17*, 1424–1433.
[11] S. Bauer, T. Bein, N. Stock, *J. Solid State Chem.* **2006**, *179*, 145–155.
[12] N. Stock, N. Guillou, J. Senker, G. Férey, T. Bein, *Z. Anorg. Allg. Chem.* **2005**, *631*, 575–581.
[13] P. Kaempfe, N. Stock, *Z. Anorg. Allg. Chem.* **2008**, *634*, 714–717.
[14] A. F. Benedetto, P. J. Squattrito, F. Adani, E. Montoneri, *Inorg. Chim. Acta* **1997**, *260*, 207–216.
[15] Z.-Y. Du, H.-B. Xu, J.-G. Mao, *Inorg. Chem.* **2006**, *45*, 9780–9788.
[16] Z.-Y. Du, H.-B. Xu, J.-G. Mao, *Inorg. Chem.* **2006**, *45*, 6424–6430.
[17] F. Adani, M. Casciola, D. J. Jones, L. Massinelli, E. Montoneri, J. Roziére, R. Vivani, *J. Mater. Chem.* **1998**, *8*, 961–964.
[18] G. B. Deacon, R. Harika, P. C. Junk, B. W. Skelton, A. H. White, *New J. Chem.* **2007**, *31*, 634–645.
[19] Z.-Y. Du, V. A. Prosvirin, J.-G. Mao, *Inorg. Chem.* **2007**, *46*, 9884–9894.
[20] Z.-Y. Du, X.-L. Li, Q.-Y. Liu, J.-G. Mao, *Cryst. Growth Des.* **2007**, *7*, 1501–1507.
[21] A. Sonnauer, C. Näther, H. A. Höppe, J. Senker, N. Stock, *Inorg. Chem.* **2007**, *46*, 9968–9974.
[22] A. Sonnauer, N. Stock, *J. Solid State Chem.* **2008**, *181*, 473–479.
[23] A. Sonnauer, N. Stock, *J. Solid State Chem.* **2008**; DOI: 10.1016/j.jssc.2008.09.006.
[24] S. S.-Y. Chui, S. M.-F. Lo, J. P. H. Charmant, A. G. Orpen, I. D. Williams, *Science* **1999**, *283*, 1148–1150.
[25] N. Stock, T. Bein, *J. Mater. Chem.* **2005**, *15*, 1384–1391.
[26] R.-B. Fu, X.-T. Wu, S.-M. Hu, J.-J. Zhang, Z. Fu, W.-X. Du, *Polyhedron* **2003**, *22*, 2739–2744.
[27] P. F. Charbonnier, R. F. H. Loiseleur, *Acta Crystallogr., Sect. B* **1977**, *33*, 3759–3761.
[28] S.-R. Fan, H.-P. Xiao, L.-P. Zhang, L.-G. Zhu, *Acta Crystallogr., Sect. E* **2004**, *60*, m1833–1835.
[29] *STOE WinXPOW version 2.11*, Stoe & Cie GmbH, Darmstadt, Germany, **2005**.
[30] D. I. Arnold, X. Ouyang, A. Clearfield, *Chem. Mater.* **2002**, *14*, 2020–2027.
[31] D. M. Poojary, B. Zhang, A. Clearfield, *J. Am. Chem. Soc.* **1997**, *119*, 12550–12559.
[32] K. Barthelet, M. Nogues, D. Riou, G. Férey, *Chem. Mater.* **2002**, *14*, 4910–4918.
[33] N. Stock, T. Bein, *Angew. Chem. Int. Ed.* **2004**, *43*, 749–752.
[34] N. Stock, T. Bein, *Solid State Sci.* **2003**, *5*, 1207–1210.
[35] *XRED version 1.19*, *X-Shape version 1.06*, *RECIPE*, *TWIN*, Stoe & Cie GmbH, Darmstadt, Germany, **1999**.
[36] G. M. Sheldrick, *SHELXTL-PLUS* Crystallographic System, Siemens Analytical X-ray Instruments Inc., Madison, WI, **1992**.

Received: March 28, 2008
Published Online: September 30, 2008

